Hand and Body Blockage Measurements With Form-Factor User Equipment at 28 GHz

Vasanthan Raghavan, *Senior Member, IEEE*, Sonsay Noimanivone, Sung Kil Rho, Bernie Farin, Patrick Connor, Ricardo A. Motos, Yu-Chin Ou, *Member, IEEE*, Kobi Ravid, Mohammad Ali Tassoudji, Ozge Hizir Koymen, *Member, IEEE*, and Junyi Li, *Fellow, IEEE*

***Abstract*— Blockage by the human hand/body is an important impairment in realizing practical millimeter-wave wireless systems. Prior works on blockage modeling are either based on theoretical studies of double knife-edge diffraction or its modifications, high-frequency simulations of electromagnetic effects, or measurements with experimental millimeter-wave prototypes. While such studies are useful, they do not capture the form-factor constraints of user equipments (UEs), such as moderate array sizes, gains, and beamwidths. In this work, we study the impact of hand/body blockage with a UE at 28 GHz built on commercial millimeter-wave components. We report five controlled studies with different types of hand holdings/grips, antenna types, and directional/narrow beams. For both hard and loose hand grips, we report considerably lower blockage loss estimates than prior works. Critical in estimating the loss is the definition of a "region of interest" (RoI) around the UE where the impact of the hand/body is seen. Toward this goal, we define an RoI that includes the spatial area where significant energy is seen in either the no blockage or blockage modes. Our studies show that significant spatial area coverage improvement can be seen with a loose hand grip due to hand reflections.**

***Index Terms*— 28 GHz, 5G new radio, body blockage, form-factor user equipment (UE), hand blockage, measurements, millimeter wave, UE design.**

I. Introduction

OVER the last ten years, the interest in millimeter-wave carrier frequencies has transformed from an academic/theoretical pursuit to commercial deployments. The first wave of commercial form-factor user equipments (UEs) is already available in the market with the physical layer operation conforming to the Third Generation Partnership Project (3GPP) standard specifications in Releases 15 and 16. Despite this essentially mature background in both the theory and practice of millimeter-wave systems (see [2] and references therein for the maturity of millimeter-wave theoretical aspects), there is still considerable and growing interest in understanding the performance limits of such systems imposed by the channel and propagation characteristics, radio frequency (RF) and hardware constraints, and their impact and implications on low-cost, low-complexity, and power-efficient physical layer design. The focus of this work is on one such impairment: blockage of millimeter-wave signals at the UE end due to human hand and body.

Given that blockage is not a dominant impairment at sub-6 GHz carrier frequencies, a number of prior works have focused on modeling blockage and understanding its implications on millimeter-wave system performance. In particular, wireless standardization efforts at 60 GHz for 802.11 (ad) Wi-Fi systems use ray-tracing studies to propose a human blockage model [3, Secs. 3.3.8, 3.5.7, 5.3.9, and 8]. This model reflects the probability that a blockage event happens, a distribution for blockage loss conditioned on it happening and time-scale modeling for blockage events. For cellular millimeter-wave systems, the 3GPP TR38.901 [4, pp. 53–57] proposes a flat 30 dB loss over a defined blockage region for the UE in either the portrait or landscape modes. The loss region is modeled using data from studies with a form-factor experimental millimeter-wave UE mock-up/prototype at 28 and 60 GHz and the loss is motivated by the[1] state-of-the-art survey of measurement studies with human/body blockage in 2015–2016. The Mobile and wireless communications Enablers for the Twenty-twenty Information Society (METIS) project has proposed a human blockage model based on the double knife-edge diffraction (DKED) framework in [5, pp. 39–41 and 160–162]. Human blockage measurements over a wideband setup at 60 GHz have been considered in [6], where comparisons are made in terms of model fitting with the DKED and the uniform theory of diffraction (UTD) frameworks. Human blockage measurements using a 73 GHz horn antenna setup is considered in [7]–[9] and substantial losses (in the range of 30–40 dB) are reported.

In terms of form-factor studies, the impact of blockage at 15 GHz in terms of the total scan pattern and coverage efficiency is studied in [10] and [11]. A similar study with

Manuscript received April 21, 2020; revised April 28, 2021; accepted June 20, 2021. Date of publication July 26, 2021; date of current version January 11, 2022. This article was presented at the Proceedings of Asilomar Conference on Signals, Systems and Computers, November 2020. *(Corresponding author: Vasanthan Raghavan.)*

This work involved human subjects or animals in its research. The authors confirm that all human/animal subject research procedures and protocols are exempt from review board approval.

Vasanthan Raghavan, Kobi Ravid, Ozge Hizir Koymen, and Junyi Li are with Qualcomm, Inc., Bridgewater, NJ 08807 USA (e-mail: vraghava@qti.qualcomm.com).

Sonsay Noimanivone, Sung Kil Rho, Bernie Farin, Patrick Connor, Ricardo A. Motos, Yu-Chin Ou, and Mohammad Ali Tassoudji are with Qualcomm, Inc., San Diego, CA 92121 USA.

Color versions of one or more figures in this article are available at https://doi.org/10.1109/TAP.2021.3098537.

Digital Object Identifier 10.1109/TAP.2021.3098537

[1]The study item on channel modeling at 3GPP was conducted in 2015–2016.

0018-926X © 2021 IEEE. Personal use is permitted, but republication/redistribution requires IEEE permission.
See https://www.ieee.org/publications/rights/index.html for more information.

ray tracing is performed in [12] for 15 and 28 GHz systems. In general, reduced losses are reported and subarray diversity is recommended for overcoming the deleterious effects of blockage. Significantly reduced body blockage losses are also reported for 28 GHz in [13] and this is attributed to creeping waves and diffraction of signals into the shadow of the user. Simulated studies of hand blockage losses with an 8×1 linear antenna array and a 10×1 irregular antenna array in a 28 GHz form-factor phone design are presented in [14] and [15], respectively. In both works, reduced blockage losses relative to the 3GPP model are reported. Terminal housing effects and impact of palm, fingertip, and so on are studied via simulations at 28 GHz and several decibels of losses are suggested. Simulation studies of blockage with a finger blocking the antenna module at 60 GHz are reported in [16] and [17] and it is noted that a finger placed close to the radiating element can severely detune it and degrade the radiation efficiency. User effects on the power variation are reported for 21.5 GHz systems in [18] with many scenarios of loss and some scenarios of gain observed. An important caveat common to most of these prior studies on blockage modeling is that they are either based on ray tracing or electromagnetic simulation studies or with experimental prototypes that may/may not be a form-factor implementation. Coverage over the sphere of different form-factor designs and their implications for good design structures are reported in [19] and [20]. Phased array versus switched diversity array tradeoffs with hand and body blockage are studied in [21] and the regime where each approach is better is quantified.

More recently, the loss with blockage is estimated in a prior work of ours [22] using a 28 GHz form-factor prototype performing real-time beam switching/management and operating according to the system-level specifications analogous to the 3GPP framework, albeit with a proprietary subframe structure. This study reported order-of-magnitude smaller blockage losses in beamformed systems than prior modeling efforts (e.g., 30 dB loss in TR38.901). In this study, blockage loss was estimated with over-the-air (OTA) measurements of beamformed received power differential between the no blockage and blockage scenarios. While such studies are useful in understanding the practical impact of blockage, the received power differential is a function of the channel environment (rich versus sparse multipath propagation) and the set of beam weights with which the link has been established between the base-station and the UE (which determines the dominant cluster in the channel excited in beamforming).

Contributions: In this context, this work reports blockage losses with a commercial form-factor UE operating at 28 GHz. The UE is equipped with a commercial-grade millimeter-wave modem and antenna module solution and driven by a beam management software solution that adheres to the 3GPP system-level protocol specifications in Releases 15 and 16 [23]. The antenna module incorporated here uses a 4×1 dual-polarized patch array and two 2×1 dipole arrays across two polarizations/layers. Multiple commercial millimeter-wave UEs available in the market today use similar antenna, modem, and system-level software implementations that realize low-overhead and low-complexity analog/RF beamforming and beam tracking [24], thereby improving signal range and coverage. Thus, this work is directly relevant in understanding blockage from a practical/implementation perspective.

In contrast to OTA measurements mentioned in [22], we report five controlled studies in an anechoic chamber that allows us to understand blockage by studying beam patterns over a sphere with freespace/no blockage and a human holding the phone with the hand and body of the human blocking the signals. By studying the beam patterns over a sphere, the impact of the channel used to establish a beamformed link is removed and we can showcase the impact of blockage in different directions. The reported studies correspond to different targeted antenna arrays of different dimensions (4×1 patch array versus 2×1 dipole array), different UE orientations (portrait versus landscape), and different hand holdings/grips. The grips studied here include a "hard" hand holding grip where the hand completely engulfs all the antenna elements in the array with minimal air gaps between the fingers, a "loose" hand holding grip where only a few fingers engulf some of the antenna elements in the array with the remaining antenna elements seeing unobstructed signals, and an "intermediate" hand holding grip where a few fingers engulf some antenna elements with a big air gap between the palm of the hand and the remaining antenna elements.

From our studies, we observe that the gross estimate of blockage losses obtained by comparing the cumulative distribution functions (CDFs) of radiated signal power with and without blockage is significantly lower than loss estimates at 3GPP [4] and in prior studies [7]–[9], [16], [17]. The estimates provided here are also consistent with (and similar to) our prior work [22] that used a 28 GHz experimental prototype as well as other measurement/simulation results reported earlier. Depending on the antenna type (dipole or patch), array size (4×1 versus 2×1), type of beam used (scan angle and beamwidth), material property of UE, and the user's hand properties (such as hand grip, hand size, and skin properties), we show that the hand and the body can either attenuate signals or amplify signals (via reflection) in specific directions. With a primary focus on blockage loss in prior works, the impact of hand reflections has not been explored. In this context, this work provides a first understanding of this aspect.

To understand the impact of hand/body, we need to define a "region of interest" (RoI) where the impact of blockage is observed. A naïve definition of the RoI corresponds to the no blockage region that is within a fixed signal threshold of its peak value. This RoI does not capture hand reflections into regions that have a poor signal strength in the no blockage mode. To capture hand reflections, we augment this region with the region where signal strength in the blockage mode is also above a signal strength threshold. We show that while the former naïve RoI is sufficient to capture the impact of blockage in scenarios with a hard hand grip where there are no prominent air gaps between fingers and, hence, there are minimal hand reflections, it is not sufficient with loose or intermediate hand grips where a few antenna elements are unobstructed or where a significant air gap can be seen between some fingers. In these scenarios, the hand grips can

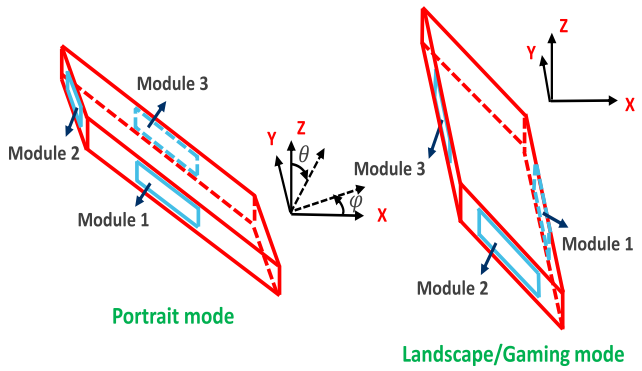

Fig. 1. Pictorial illustration of the relative positions of the three antenna modules in the portrait and landscape modes from a side view of the UE [19]. Reference coordinate system for the measurements is also presented.

lead to reflection gains and the enhanced RoI is necessary to capture the impact of blockage.

This article is organized as follows. Section II explains the experimental setup considered in this work in terms of hand/body blockage measurements. Section III considers the 4×1 patch subarray with a hard hand grip and studies the impact of hand/body blockage in careful detail by exploring the different RoI definitions in understanding the implications of blockage. Section IV performs similar studies for the four other scenarios considered in this work. Section V develops models for blockage for all the five scenarios considered here as well as compares the physical layer implications of this work with prior models on blockage. Section VI concludes this article. In terms of notations, we use the term "beam pattern" and "beamforming gain" to denote the array gain with a single set of beam weights over the antenna array and the best of multiple sets of beam weights over the array, respectively.

II. Experimental Setup

We now explain the experimental setup used for measuring hand/body blockage in this article.

A. User Equipment

The UE used in this study is equipped with a millimeter-wave modem operating at 28 GHz and using a 3GPP Releases 15 and 16 spec-compliant software solution that performs intelligent beamforming and beam tracking. The details of the design of transmit–receive front ends and packaging aspects in the design of antenna arrays would take us on a tangent to the scope of the discussion in this article. More details on these aspects can be found in [19] and [25]–[27]. From an antenna module perspective, the UE consists of three modules denoted as Modules 1–3. These modules are equipped on the three edges/sides (two long edges and the top short edge) of the UE. Each antenna module has a 4×1 dual-polarized patch array as well as two 2×1 dipole arrays that allow dual-polarized transmissions via two RF chains at 28 GHz (see Fig. 1, [19] for an illustration of the UE in both the portrait and landscape modes). The arrows in Fig. 1 are just pointers to the antenna modules and do not correlate with the boresight directions of the arrays. Since the UE is a precommercial design, it has a width beyond 72 mm making it a wide-body phone design.

B. Chamber Measurement Setup

The anechoic chamber setup used for measurements is now described. The measurement (receiving) antenna is an off-the-shelf dual-polarized broadband horn antenna (covering 18–40 GHz) with an antenna gain of ≈14 dBi at 28 GHz. The 3 dB beamwidth in the H- and E-planes of the horn antenna at 28 GHz are 25.8° and 31.9°, respectively. The UE is placed on a fiberglass pedestal in the center of the chamber. The transmit power used with the active millimeter-wave antenna module is 4 dBm, which is well within the 3GPP effective isotropically radiated power (EIRP) regulations for commercial millimeter-wave devices and is intended for short-distance coverage between the UE and the measurement antenna. The distance between the UE and the measurement antenna is ≈1.50 m (59 in).

Short RF flex cables (with some loss) are used to connect the measurement antenna with a power meter. The power level observed by the power meter (P_{rx}) can be written as

$$\mathsf{P}_{\mathsf{rx}} = \mathsf{P}_{\mathsf{tx}} + G_{\mathsf{rx}} - \mathsf{Path\ loss} - \mathsf{Loss}_{\mathsf{cable}}$$

where P_{tx} is the transmitted power with reference plane set to the outer surface of the back cover[2] of the UE side, G_{rx} is the gain of the measurement antenna, and $\mathsf{Path\ loss}$ and $\mathsf{Loss}_{\mathsf{cable}}$ correspond to loss in OTA transmissions (with a path loss exponent of 2.0 since a line-of-sight path is maintained between the UE and the measurement antenna) and loss in the cables connecting the horn antenna with the power meter, respectively. To measure the received power level accurately, an OTA path loss calibration procedure is performed to capture the impact of measurement antenna gain, cable loss, and path loss. Note that while P_{tx} can be estimated theoretically, measurements are needed to understand the over-estimation/underestimation of single-antenna elemental gains and the array gains due to different sets of beam weights in different directions, as well as nonidealities in the array geometry and impact of UE material properties on the observed beam patterns.

As the UE transmits with a certain set of beam weights, the measurement antenna is rotated (control for the rotation is driven by an automated software) at ≈5° steps in azimuth and elevation. Due to the design of the chamber, a limited 170° (of the possible 180°) coverage in the elevation plane is possible leading to a coverage map of the beam pattern over the 360° × 170° part of the sphere. By carefully choosing the UE orientation without and with blockage, the impact of the missing 10° in elevation plane on the conclusions of this work can be made minimal. In the tests conducted in this article, the UE orientation in the testing positions means that the missing 10° is toward the bottom of the UE, which has no antenna module coverage and is covered by sidelobes of other antenna modules. Since the EIRP in these sidelobe directions

[2]The considered reference plane implies that the loss due to the radome/back cover is lumped with the measured data, and thus, it is not necessary to worry about the angle-dependent radome loss.

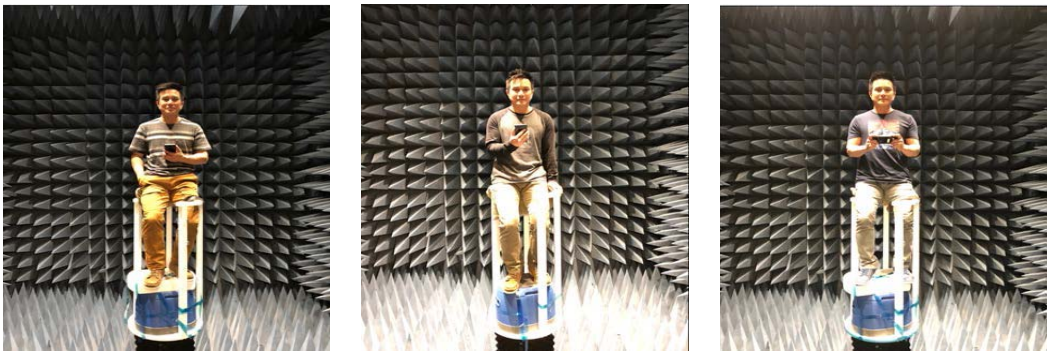

(a) (b) (c)

Fig. 2. Illustration of a person holding the UE on (a) left-hand side and (b) right-hand side, both in portrait mode and (c) in gaming/landscape mode.

is expected to be considerably low, lack of measurements in the missing 10° is expected to affect the tail of the performance curves, which do not carry any major impact on understanding the implications of blockage.

C. Setup of Hand Holding Tests

For the hand holding tests, a testing person holds the UE in the portrait and landscape modes as shown in Fig. 2 and sits in a static position in the chamber, while the measurements are conducted. Each test (scan over the sphere) takes approximately 18–21 min, and thus, different testing persons are employed in the studies in this article. The testing persons vary from having a small body size (65.8 kg, 1.63 m and 74.8 kg, 1.55 m) to a large body size (97.1 kg, 1.85 m). In general, blockage losses could be a function of size of the hand, palm, and fingers as well as skin properties of the hand, type of hand holding/grip, and steering direction of the beams (also see [22]).

In terms of hand holding, three broad categories of tests are identified.

1) A hard hand grip with the right hand in the portrait mode that completely engulfs all the antenna elements in Module 3 with no air gaps between the fingers, and no air gaps between the fingers and the radiating elements.
2) A loose hand grip with the left hand in the portrait mode where only a few fingers engulf some of the antenna elements in Module 3 with unobstructed signals from other antenna elements. A few millimeters of air gap between fingers (on the order of 1–2 mm) are observed for Module 3. While signals are blocked out of Module 1 with the left hand holding (which sees a hard hand grip mode), we focus on the opposite edge module (Module 3) that sees a lesser impact on the hand and fingers.
3) An intermediate hand grip with two hands in the landscape mode where a few fingers engulf some antenna elements in Module 2 with a big air gap (more than 5 mm) between the palm of the hand and the remaining antenna elements. The air gap between the fingers is again on the order of 1–2 mm.

Under this broad categorization of hand holdings, five studies with summary statistics capturing the subarray type/size/configuration, UE orientation, and type of hand grip are described in Table I. These five studies include a diversity of subarrays (4×1 versus 2×1), hard, loose, as well as intermediate hand grips, and both portrait and landscape/gaming modes. Sections III and IV will focus on these five studies in more detail.

TABLE I
SUMMARY OF THE PARAMETERS IN THE CONSIDERED BLOCKAGE SCENARIOS

Study	Subarray type	UE orientation	Hand grip
1	4×1 patch	Portrait	Hard
2	4×1 patch	Portrait	Loose
3	2×1 dipole	Portrait	Hard
4	2×1 dipole	Portrait	Loose
5	4×1 patch	Landscape	Intermediate

The deployment of multiple antennas at millimeter-wave carrier frequencies can be leveraged to improve the link margin via beamforming. Since a limited number of RF chains are available at the UE end at millimeter-wave carrier frequencies (the UE considered in this work has two RF chains, which are used for polarization-based transmissions), increased received power is realized with analog/RF beamforming. Here, a 3 bit phase shifter and a variable gain amplitude control are used at each antenna element to cophase the signals along the desired/prespecified set(s) of directions. A beamforming scheme realized with a finite-sized analog/RF beam codebook of beam weights that steers energy along the dominant cluster(s) in the channel is a good low-complexity near-optimal solution relative to the optimal beamforming scheme (performing maximum ratio combining) [24], [28]. The performance of this codebook improves as the codebook size increases and approaches the performance of a directional beamforming scheme with perfect knowledge of the dominant cluster in the channel as seen at the base station and UE ends [28].

III. STUDY 1: 4×1 PATCH SUBARRAY WITH A HARD HAND GRIP

In this section, we study the beamforming performance of the analog codebook of beams (without/with blockage) for the

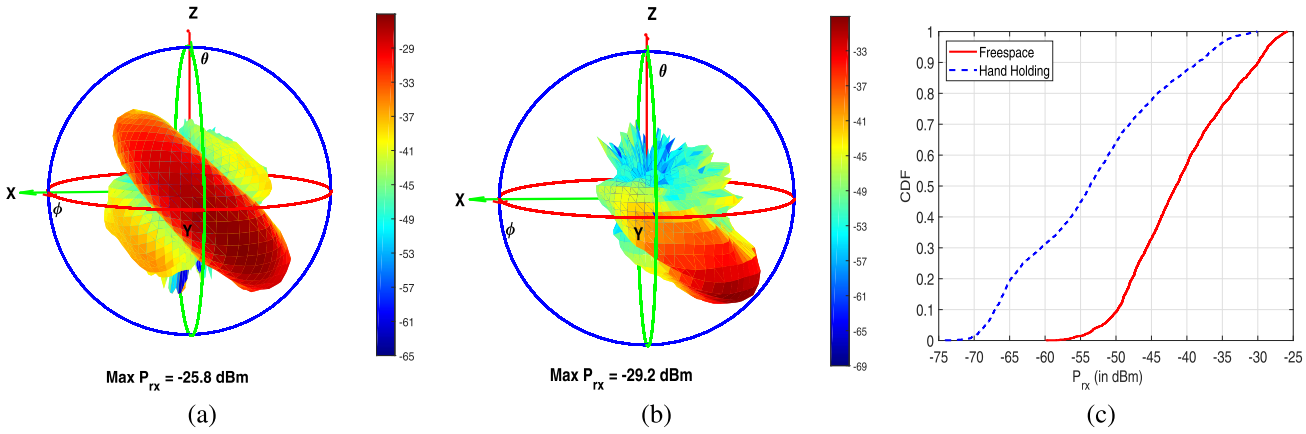

Fig. 3. Beam patterns (a) without and (b) with hand holding for a certain beam considered for the 4×1 patch subarray. The intended boresight direction of all the three beams in freespace are in the XY plane and perpendicular to the plane with the paper. (c) CDFs of $\mathsf{P_{rx}}$ for different modes in the 4×1 patch subarray.

4×1 patch subarray in Module 3 with a hard hand grip. Other subarrays and hand holdings are considered in Section IV.

A. Received Power With Beamforming

To understand the implications of blockage, we consider a codebook of three beams for the 4×1 subarray. We consider a small codebook size of three since practical UE codebook constraints are determined by low-latency requirements for initial link acquisition [24] and low power consumption, which requires a small codebook size. In the case of the 4×1 patch subarray, these three beams are chosen to steer energy along the boresight of the array, $+30°$ to the boresight, and $-30°$ to the boresight. The received power without blockage for the boresight beam over a sphere around the UE (reflecting its beam pattern) is shown in Fig. 3(a). Note that in addition to the correct orientation of the beam pattern (relative to the coordinate system in Fig. 1), the beam pattern is close to the theoretically expected performance of the beam pattern of a progressive phase shift set of beam weights [29]. Furthermore, the beamwidth of the beam is $\approx$25°–30°, suggesting that the three beams can cover a 75°–90° spatial area in one dimension, which is typically the coverage area of a linear array at millimeter-wave carrier frequencies.

In a beamformed realization, an overlay plot of the beam pattern over the sphere due to the best of the three beams (which we denote as the "received power with beamforming using the best of the three beam weights") is important. This is because the UE could switch between the three available beams based on the angle of arrival of the dominant cluster in the channel and by measuring the best received power over a reference signal [23]. Such a characterization, by way of comparison without and with blockage, also allows us to understand the impact of blockage on beamformed performance. Fig. 4(a) shows this overlay plot for the 4×1 patch subarray without blockage. In this plot, the behavior over the sphere is plotted as a 2-D plane (over ϕ–θ where ϕ and θ are the azimuth[3] and zenith angles, respectively). From this plot, we observe that this subarray is well-designed to ensure good coverage over at least a $90° \times 60°$ coverage region without blockage, which is typical for antenna arrays at millimeter-wave carrier frequencies.

We next consider the behavior of the beam weights used with the patch subarray with the hand holding the UE. Fig. 3(b) plots the beam pattern of the boresight beam in this setup. The received power with beamforming using the best of three beam weights is plotted in Fig. 4(b). Note that Fig. 4(b) shows that the impact of the beam, which is at $-30°$ off boresight, is rarely observed in the overlay plot.

From these plots, the distortion with the hand holding is significant with considerable signal deterioration observed over the three beam patterns without blockage (notably, peak $\mathsf{P_{rx}}$ distortion of 3.4, 2.9, and 8.6 dB for the three beams). Specifically, the beam that is $+30°$ off boresight steers energy toward the torso, hips, and stomach of the human holding the UE and is thus less impacted in terms of signal distortion relative to the beam that is $-30°$ off boresight, which steers energy toward the face and shoulder and is thus significantly impacted by the human.

B. Estimating the Loss Region

To understand the implications of beamforming, we now plot the CDFs of $\mathsf{P_{rx}}$ as seen over the sphere (weighted by $\sin(\theta)$) without and with blockage. The weighting by $\sin(\theta)$ is essential since the sample points in the ϕ–θ plane are uniform (at steps of 5°) leading to crowding of points near the poles, which needs to be adjusted by the Jacobian of the coordinate transformation from a Cartesian/rectangular coordinate system to a spherical coordinate system [19]. First, note that from the link budget analysis in Section II-B, the range of $\mathsf{P_{rx}}$ is below -25 dBm in Fig. 3(c). Furthermore, the plot in Fig. 3(c) shows that there are two ways to interpret the CDF data. In the first view, the hand holding leads to a 20%–45% absolute[4] spherical

[3]Note that as shown in Fig. 1, θ denotes the angle between the Z-axis and the point of interest in the direction towards the XY plane, and ϕ denotes the angle from the X-axis towards the point of interest over the XY plane.

[4]Absolute spherical coverage loss is defined as the difference of the fraction of the sphere that is above a certain $\mathsf{P_{rx}}$ threshold without and with blockage. The relative fraction of this loss in coverage (ratio of the difference with respect to the no blockage spherical coverage) is the relative spherical coverage loss.

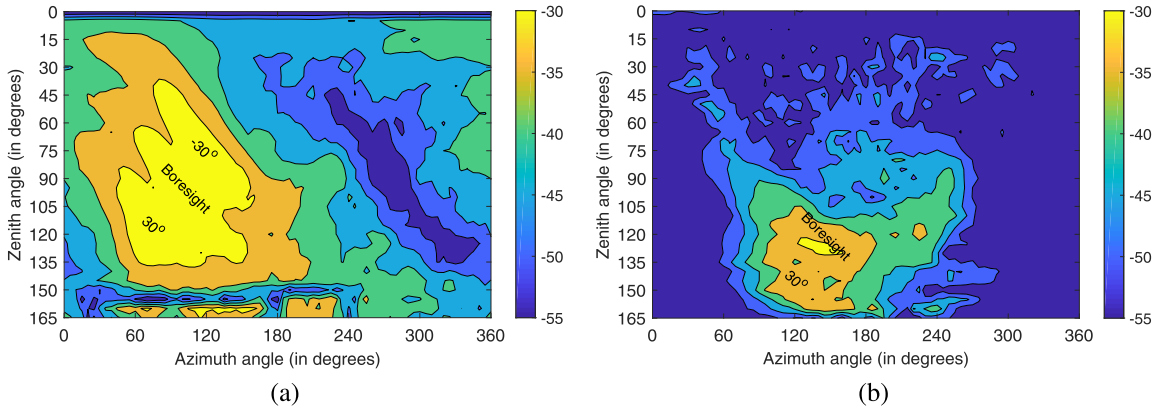

Fig. 4. Received power with beamforming using the best of the three beam weights (a) without and (b) with hand holding for the 4×1 patch subarray. Labels on colorbar indicate P_{rx} values (in dBm).

TABLE II

RECEIVED POWER-BASED COMPARISONS FOR THE HARD HAND GRIP (STUDY 1)

P_{rx} (in dBm)	Spherical Cov. Freespace (in %)	Spherical Cov. Hand (in %)	Spherical Cov. Lost (in %) Abs.	Spherical Cov. Lost (in %) Rel.	%ile	Loss (in dB)
> -35	23.3	3.4	19.8	85.3	80	10.6
> -40	41.8	12.1	29.7	71.0	50	12.2
> -45	65.0	21.7	43.4	66.7	20	17.2

coverage loss at different P_{rx} levels. In the second view, the hand leads to a signal strength degradation of 8.5–17 dB at different percentile points. Table II provides a summary of the actual spherical coverages without and with blockage as well as the absolute and relative spherical coverage losses at different P_{rx} levels. A complementary view of the losses seen at different percentile points is also presented.

Given such a wide range of losses at different percentile points, it is reasonable to ask as to what is a good model for spherical coverage loss and/or blockage loss. We now deal with this question in more detail. To understand the impact of blockage, two broad questions can be laid out.

1) What is the RoI in terms of blockage's impact?
2) What is the loss seen over this RoI? Can this loss be modeled by an appropriate stochastic distribution?

Simply selecting the entire sphere as the RoI is unreasonable since antenna arrays/modules at millimeter-wave frequencies have limited spatial coverage with poor EIRPs beyond the coverage region. In any case, in the sequel, we show that the above view is quite simplistic in terms of characterizing blockage behavior. Specifically, we show that blockage does not just lead to losses over the RoI but can also lead to gains due to reflection of signals from fingers, palm, and hand. The precise nature and scale of the reflection gains depends on the type of hand grip and orientation, user-specific skin properties, and so on. Thus, to truly understand the implications of blockage in terms of physical layer performance, we need to define the RoI carefully. Toward this goal, we define a different RoI and show the broad utility of these two specific RoI definitions.

Let $G(\theta, \phi)$ denote the received power with beamforming (in dBm) with a certain set of beam weights as seen without blockage in a certain direction (θ, ϕ). Let G_{max} (also in dBm) denote the maximum gain without blockage over all directions, i.e.,

$$G_{\mathsf{max}} = \max_{\theta,\phi} G(\theta, \phi).$$

Also, let $G_{\mathsf{body}}(\theta, \phi)$ and $G_{\mathsf{max,body}}$ denote the received power with beamforming seen with hand holding the UE (i.e., hand/body blockage) in a direction (θ, ϕ) and the maximum of this gain over all (θ, ϕ).

The typical definition of an RoI for a certain choice of threshold Δ_1 (in dB) is

$$\mathcal{R}_1(\Delta_1) = \{(\theta, \phi) : G(\theta, \phi) \geq G_{\mathsf{max}} - \Delta_1\}$$

that is, $\mathcal{R}_1(\Delta_1)$ captures the region where the gains without blockage are within a fixed cutoff (Δ_1 dB) of G_{max}. It is important to note that this definition of $\mathcal{R}_1$ only relies on the freespace gain and not on what happens with hand/body blockage (which is quite naïve from understanding the implications of blockage). Furthermore, this region does not have to be a rectangular/regular region in (θ, ϕ) nor does it have to be a single connected region. In general, $\mathcal{R}_1(\Delta_1)$ could be a union of multiple irregular regions.

By noting that $\mathcal{R}_1$ does not entirely capture blockage behavior and only freespace performance, our objective is to augment $\mathcal{R}_1$ with parts of the sphere where blockage can lead to reflection gains. This objective can be realized in many ways. A natural candidate is to consider an augmented region where $G_{\mathsf{body}}(\theta, \phi) > G(\theta, \phi)$. However, this constraint is typically pessimistic by expecting blockage behavior to be better than freespace performance and is therefore not considered here. As an alternative, we define

$$\mathcal{R}_2(\Delta_2) = \{(\theta, \phi) : G(\theta, \phi) \text{ or } G_{\mathsf{body}}(\theta, \phi) \geq \Delta_2\}$$

for an appropriate choice of Δ_2. It is important to note that the units of Δ_2 are dBm (corresponding to thresholds on P_{rx} with blockage), whereas the units of Δ_1 are in dB. The intuitive meaning of $\mathcal{R}_2$ is that in addition to the region captured by $\mathcal{R}_1$, $\mathcal{R}_2$ captures the region where either freespace- or hand/body

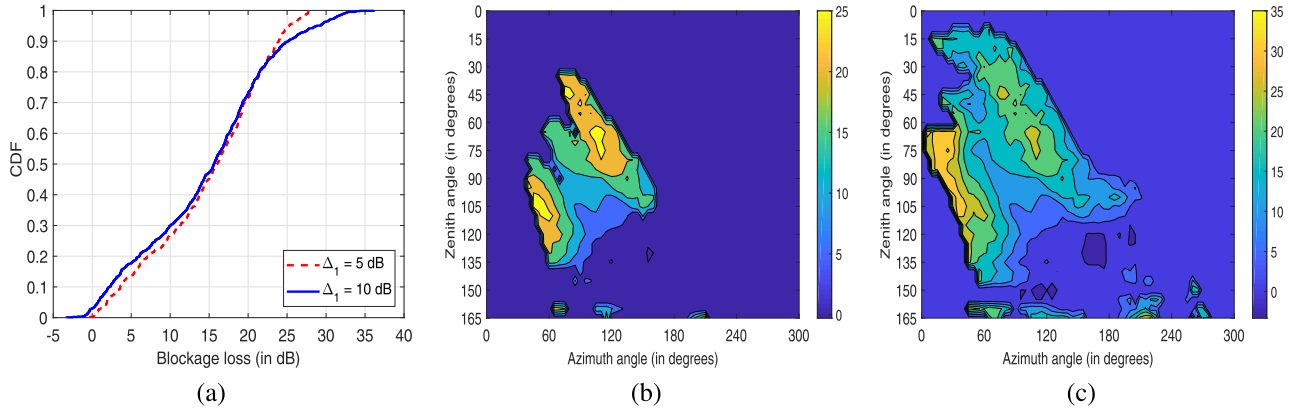

(a) (b) (c)

Fig. 5. (a) Blockage loss with the hard hand grip over $\mathcal{R}_1$ with $\Delta_1 = 5$ and 10 dB. Blockage behavior over the sphere with the hand holding for $\mathcal{R}_1$ with (b) $\Delta_1 = 5$ dB and (c) $\Delta_1 = 10$ dB. Labels of colorbar indicate blockage loss (in dB).

blockage-based signals are good as described by the common link margin threshold Δ_2 (which is chosen to meet some link budget constraint).

The RoI $\mathcal{R}_1$ with $\Delta_1 = 5$ dB and $\Delta_1 = 10$ dB captures $\approx$14.6% and $\approx$32.6% of the sphere, respectively. It is clear that as we increase Δ_1, we will eventually capture the entire sphere and, by default, also incorporate those directions where hand reflection gains are substantial. However, $\mathcal{R}_1$ with a large value for Δ_1 and a subsequent focus on the entire/substantial portion of the sphere in a millimeter-wave system with multiple antenna modules covering limited portions of the sphere is an artificial approach to understand the impact of blockage. A more natural approach is to consider a small value for Δ_1 (e.g., 5 or 10 dB) and study the enhancement of $\mathcal{R}_2$ over $\mathcal{R}_1$. In terms of relationships across the RoIs, by definition, we have $\mathcal{R}_1(\Delta_1) \subset \mathcal{R}_2(\Delta_2)$ if $\Delta_2 \leq G_{\text{max}} - \Delta_1$. In the $\Delta_2 > G_{\text{max}} - \Delta_1$ setting, whether $\mathcal{R}_2$ is bigger than $\mathcal{R}_1$ (or not) depends on the actual gain relationships.

In terms of choices of Δ's, from a beam management perspective, switching from a cluster in the channel with a (hypothetical) peak $\mathsf{P_{rx}}$ to a different cluster that is Δ_1 dB away is acceptable without significant performance loss as long as Δ_1 is small. Choices, such as $\Delta_1 = 5$ or 10 dB, serve as good example parameters. The latter choice of 10 dB leads to a focus on approximately one-third of the sphere, which closely approximates the three-module capability for which the UE's beam management solution has been designed for.

The received SNR seen by the UE side in downlink beamforming can be written as

$$\mathsf{SNR_{rx}} = \mathsf{P_{tx}} + G_{\mathsf{rx}} - \mathsf{MAPL} - \text{Noise power}$$
$$\implies G_{\mathsf{rx}} = \mathsf{SNR_{rx}} - \mathsf{P_{tx}} + \mathsf{MAPL} + \text{Noise power}$$

where MAPL denotes the maximum allowed path loss for the link under consideration. Thus, a threshold on G_{rx} is equivalent to a threshold on the received SNR assuming a certain allowed MAPL, noise sensitivity at the receiver, and EIRP at the transmitter. These system-level parameters determine what thresholds are appropriate for Δ_2. In our study, choices for Δ_2 ranging from -35 dBm (in 5 dB steps) up to -55 dBm appear to be reasonable.

We now present the CDFs of the received power differential between the without and with blockage scenarios (blockage loss) for the RoI corresponding to $\mathcal{R}_1$ with $\Delta_1 = 5$ dB and $\Delta_1 = 10$ dB in Fig. 5(a). The mean, median, and standard deviation of the loss with hand holding are 14.9, 16.0, and 7.3 dB in the former case and 14.7, 15.6, and 8.4 dB in the latter case. Furthermore, the blockage loss over these regions based on the beamforming gain of the best of the three beams is plotted in the ϕ–θ plane in Figs. 5(b) and (c). Clearly, these plots show that the hand holding behavior seen over $\mathcal{R}_1$ is mostly loss, which is typical of blockage loss characterization in prior works. However, as shown in Fig. 5(c) and as stated before, a focus on a large portion of the sphere ensures that negative blockage losses (or reflection gains) are also seen over some parts of the sphere. A better way to capture these gains is via $\mathcal{R}_2$. In this case, Fig. 6 shows a representative plot of blockage loss with some choices of parameters defining $\mathcal{R}_2$. From these plots, we observe that there are some regions of the sphere where hand reflections can lead to substantial gains (regions marked by ellipses in Fig. 6). Based on the new RoI definition, the mean, median, standard deviation of blockage loss, and the RoI's coverage area in the sphere are described in Table III.

Note that $\mathcal{R}_1$ corresponds to the RoI with just freespace information alone, whereas $\mathcal{R}_2$ corresponds to freespace as well as hand/body information. In general, we are interested in performing a head-to-head comparison between these two RoIs as they generally capture how RoI is defined in prior works and how RoI can be modified by incorporating blockage information. For this head-to-head comparison, we choose Δ_1 and $\Delta_2 = G_{\text{max}} - \Delta_1$ to ensure that the EIRP is below a fixed level in both cases (in this comparison, we choose $\Delta_2 = -35$ and -40 dBm as benchmarks). Table IV compares $\mathcal{R}_1$ with $\mathcal{R}_2$ and quantifies how big an augmentation $\mathcal{R}_2$ is with respect to $\mathcal{R}_1$. The intuition here is that a smaller augmentation means that the hand does not reflect energy that much more than we anticipate and a larger augmentation means that the hand indeed enhances the signal energy seen over the sphere in contrast to what the no blockage performance is. Table IV shows that $\mathcal{R}_2$ only improves the area of interest on an absolute scale by 1%–2.5% (relatively from 2% to 4.5%) of the sphere.

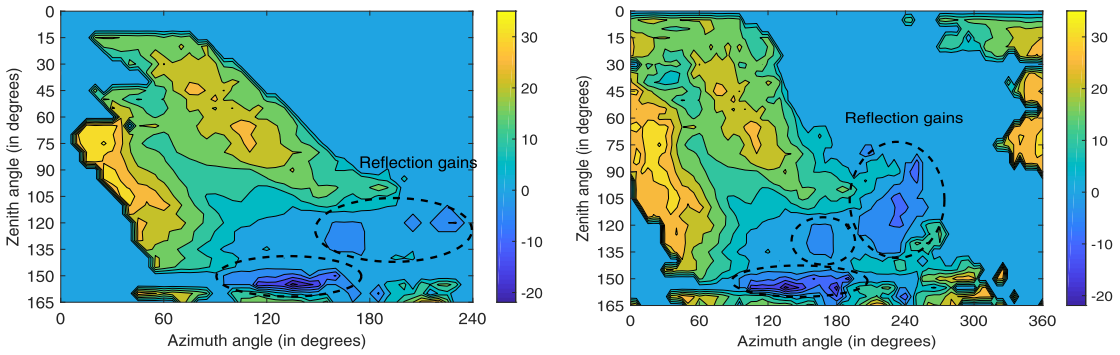

Fig. 6. Blockage loss with the hard hand grip over $\mathcal{R}_2$ with (a) $\Delta_2 = -35$ dBm and (b) $\Delta_2 = -40$ dBm. Labels on colorbar indicate blockage loss (in dB).

TABLE III
BLOCKAGE LOSS STATISTICS OVER DIFFERENT ROIS FOR THE HARD HAND GRIP (STUDY 1)

Criterion	Mean (in dB)	Median (in dB)	Std. deviation (in dB)	Percentage of sphere
$\mathcal{R}_1$, $\Delta_1 = 5$ dB	14.9	16.0	7.3	14.6
$\mathcal{R}_1$, $\Delta_1 = 10$ dB	14.7	15.6	8.4	32.6
$\mathcal{R}_2$, $\Delta_2 = -35$ dBm	13.9	15.4	9.2	30.8
$\mathcal{R}_2$, $\Delta_2 = -40$ dBm	14.2	15.4	9.9	57.2
$\mathcal{R}_2$, $\Delta_2 = -45$ dBm	13.7	14.1	9.6	81.8

TABLE IV
COMPARISON BETWEEN $\mathcal{R}_1$ AND $\mathcal{R}_2$ (STUDY 1)

P_{rx} (in dBm)	$\mathcal{R}_1$				$\mathcal{R}_2$				Improvement	
	Mean (in dB)	Median (in dB)	Std. dev. (in dB)	% of sph. (in %)	Mean (in dB)	Median (in dB)	Std. dev. (in dB)	% of sph. (in %)	Abs. (in %)	Rel. (in %)
> -35	14.7	15.6	8.3	29.7	13.9	15.4	9.2	30.8	1.1	3.7
> -40	15.1	15.7	8.9	54.7	14.2	15.4	9.9	57.2	2.5	4.6
> -45	14.1	14.3	9.1	80.1	13.7	14.1	9.6	81.8	1.7	2.1

This is not a substantial increase in coverage area and the reason for this small increase is that there are hardly any reflection gains in the hard hand grip mode over any part of the sphere. Thus, in this case, $\mathcal{R}_1$ *is sufficient to capture blockage loss*. However, we will see in Section IV that $\mathcal{R}_2$ and other RoIs become useful with looser hand grips.

IV. BEAMFORMING PERFORMANCE OF OTHER SUBARRAYS AND HAND HOLDINGS

We now follow along the methodology described in Section III and present the results from Studies 2–5 that cover other subarrays and hand holdings.

A. Study 2: 4×1 Patch Subarray With a Loose Hand Grip

We start with the same 4×1 patch subarray in Module 3 (as in Study 1), but with a left hand holding, which ensures that only a few fingers cover the antennas in the module. As a result, we see blockage behavior with an essentially loose hand grip mode.

Fig. 7(a) shows the overlay plot of the received power with beamforming using the best of the three beams over this subarray in the loose hand grip mode. The close similarity between this plot and the freespace plot in Fig. 4(a) suggests that the impact of the loose hand grip on blockage loss is significantly smaller than in the hard hand grip mode. Reflecting this observation, the CDF comparison of P_{rx} in Fig. 7(b) and Table V shows that 10%–25% of the spherical coverage are lost at different P_{rx} levels or an equivalent 3.5–10.5 dB loss at different spherical coverage levels. The corresponding

TABLE V
RECEIVED POWER-BASED COMPARISONS FOR STUDIES 2–5

	P_{rx} (in dBm)	Sph. Cov. Freesp. (in %)	Sph. Cov. Hand (in %)	Sph. Cov. Lost (in %) Abs.	Sph. Cov. Lost (in %) Rel.	%ile	Loss (in dB)
Study 2						90	3.7
	> -35	23.3	13.1	10.2	43.9	80	3.6
	> -40	41.8	26.8	15.0	36.0	50	5.4
	> -45	65.0	40.7	24.3	37.4	20	10.6
Study 3						90	15.9
	> -40	35.3	0.0	35.3	100.0	80	16.3
	> -45	58.9	0.7	58.2	98.8	50	15.9
	> -50	84.1	7.7	76.4	90.8	20	19.7
Study 4						90	0.4
	> -40	35.3	26.2	9.1	25.7	80	1.5
	> -45	58.9	47.1	11.8	20.0	50	2.6
	> -50	84.1	64.5	19.5	23.2	20	10.8
Study 5						90	12.7
	> -45	28.7	0.04	28.7	99.9	80	12.4
	> -50	50.3	7.6	42.8	85.0	50	10.9
	> -55	70.7	22.2	48.5	68.6	20	9.5

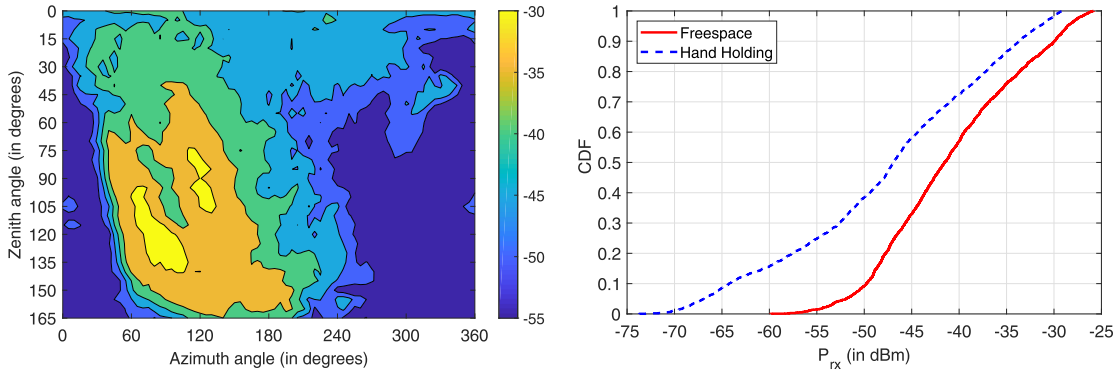

(a) (b)

Fig. 7. (a) Received power with beamforming using the best of the three beam weights for the 4×1 patch subarray in the loose hand grip mode (Study 2). Labels on colorbar indicate $\mathsf{P_{rx}}$ values (in dBm). (b) CDFs of $\mathsf{P_{rx}}$ in the 4×1 patch subarray with loose hand grip.

TABLE VI
BLOCKAGE LOSS WITH $\mathcal{R}_1$ AND $\mathcal{R}_2$ FOR STUDIES 2–5

	$\mathsf{P_{rx}}$ (in dBm)	$\mathcal{R}_1$ Mean (in dB)	$\mathcal{R}_1$ Median (in dB)	$\mathcal{R}_1$ Std. dev. (in dB)	$\mathcal{R}_1$ % of sph. (in %)	$\mathcal{R}_2$ Mean (in dB)	$\mathcal{R}_2$ Median (in dB)	$\mathcal{R}_2$ Std. dev. (in dB)	$\mathcal{R}_2$ % of sph. (in %)	Improvement Abs. (in %)	Improvement Rel. (in %)
Study 2	> -35	5.1	4.1	4.6	29.7	4.2	3.8	5.9	31.7	2.0	6.7
	> -40	7.5	5.3	7.5	54.7	6.4	4.7	8.6	58.4	3.7	6.8
	> -45	7.3	4.9	8.1	80.1	5.8	4.3	9.4	86.5	6.4	8.0
Study 3	> -40	19.3	18.4	8.1	51.3	19.3	18.4	8.1	51.3	0	0
	> -45	18.6	18.2	8.0	72.7	18.6	18.2	8.0	72.7	0	0
	> -50	17.7	17.6	8.0	87.1	17.2	17.3	9.0	88.6	1.5	1.7
Study 4	> -40	3.7	0.4	7.5	51.3	1.5	0.04	10.4	57.9	6.6	12.9
	> -45	4.8	0.8	8.3	72.7	2.9	0.4	10.5	80.5	7.8	10.7
	> -50	5.1	1.3	8.4	87.2	3.4	0.7	10.4	94.6	7.4	8.5
Study 5	> -45	18.3	18.4	5.6	39.5	15.9	17.9	9.5	43.0	3.5	8.9
	> -50	14.9	16.6	7.8	63.9	11.3	15.5	11.8	73.9	10.0	15.7
	> -55	13.1	14.6	8.4	81.8	10.5	13.6	11.3	90.8	9.0	11.0

numbers for the hard hand grip are 20%–45% and 8.5–17 dB, showing that the hand grip has a significant impact on the blockage loss observed. To understand the efficacy of an enhanced blockage region such as $\mathcal{R}_2$, we perform the same head-to-head comparison between these two RoIs as in the hard hand grip case. Table VI shows that unlike the hard hand grip case where only 1%–2.5% improvement in spherical coverage was observed with $\mathcal{R}_2$ over $\mathcal{R}_1$, we observe a 2%–6.5% improvement in absolute spherical coverage with $\mathcal{R}_2$, which is relatively more substantial. The primary reasons for this enhancement are the gains with hand reflections that are captured by $\mathcal{R}_2$, but not with $\mathcal{R}_1$, illustrating the need for such an enhanced RoI definition.

B. Study 3: 2×1 *Dipole Subarray With a Hard Hand Grip*

We now consider the beamformed performance of the 2×1 dipole array (in Module 3) with a hard hand grip. For the dipoles, we again consider a codebook of three beams steering energy toward the boresight of the array, $+45°$ to the boresight, and $-45°$ to the boresight. The change from $\pm 30°$ for the 4×1 subarray to $\pm 45°$ for the 2×1 subarray is due to beamwidth differences for different sized arrays. The beam patterns of these three beams without blockage appear regular (not illustrated here pictorially due to space constraints) with the beamwidth of each beam being $\approx 40°$–$45°$ (which is as expected for a 2×1 subarray [29]). The beam patterns with the hand show significant distortions (again not illustrated pictorially).

Reflecting these observations, the received power with beamforming using the best of three beam weights is plotted in Fig. 8(a), which shows a small ocean of yellow (or high signal strength regions). In comparison, the CDFs of $\mathsf{P_{rx}}$ in Fig. 8(b) show an almost constant gap of ≈ 15 dB between the without and with blockage performance. More precisely, Table V shows that 35%–75% of the spherical coverage are lost at different $\mathsf{P_{rx}}$ levels or an equivalent 15–20 dB loss at different spherical coverage levels. As with the patches case, $\mathcal{R}_2$ does not seem to bring in any additional value over $\mathcal{R}_1$, showing that hand reflections are not important with the hard hand grip.

C. Study 4: 2×1 *Dipole Subarray With a Loose Hand Grip*

In the loose hand grip mode, the 2×1 dipole subarray shows a similar behavior as the 4×1 patch subarray with a loose hand grip (Study 2). At different $\mathsf{P_{rx}}$ levels, a 9%–20% spherical coverage is lost relative to the no blockage case corresponding to a 0–11 dB blockage loss at different spherical coverage levels. In contrast to the hard hand

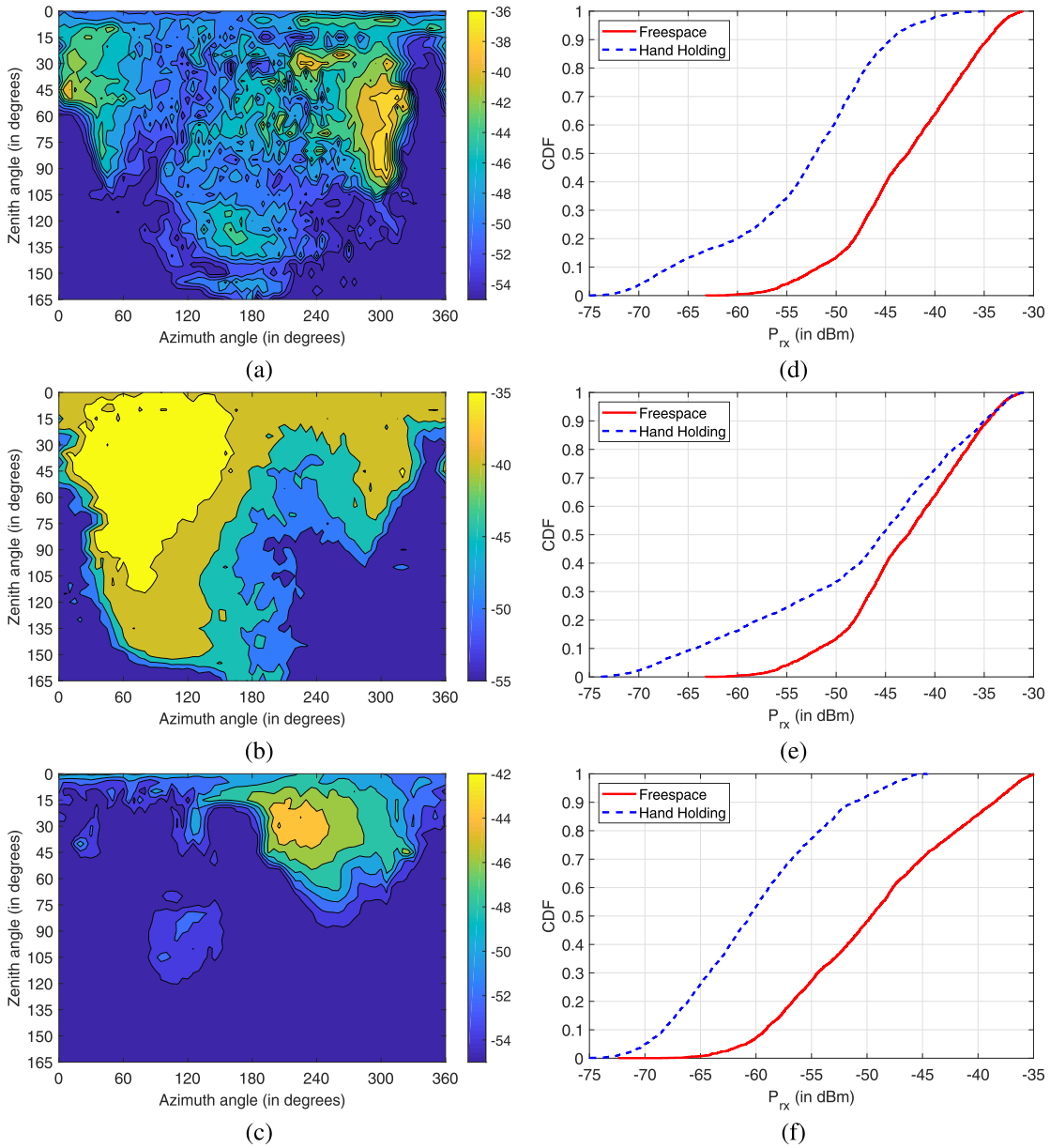

Fig. 8. (a)–(c) Received power with beamforming using the best of the three beam weights in freespace for Studies 3–5. Labels on colorbar indicate $\mathsf{P_{rx}}$ values (in dBm). (d)–(f) CDFs of $\mathsf{P_{rx}}$ with different hand modes in Studies 3–5.

grip case, we see that $\mathcal{R}_2$ can result in substantial coverage improvement over $\mathcal{R}_1$ (of 6.5%–8% absolute improvement or 8.5%–13% relative improvement). This study shows that hand reflections with loose hand grips need to be carefully captured with RoI such as $\mathcal{R}_2$ and an RoI such as $\mathcal{R}_1$, which is not sufficient in such scenarios.

D. Study 5: 4×1 *Patch Subarray With an Intermediate Hand Grip*

In the final study, a two-handed grip in the landscape mode over the 4×1 patch subarray is considered. This is an important use case in 5G communications corresponding to either gaming mode or watching videos. This study shows some effects observed with the hard hand grip as well as some effects observed with the loose hand grip studies and is thus interesting due to the complementary trends observed prior to this study. In terms of $\mathsf{P_{rx}}$ losses, we see a loss of 9.5–13 dB at different spherical coverage levels, which is equivalent to a spherical coverage loss of 25%–50% at different $\mathsf{P_{rx}}$ levels. This observation is similar to those made in the hard hand grip cases (Studies 1 and 3). On the other hand, mirroring Studies 2 and 4 (loose hand grip cases), $\mathcal{R}_2$ leads to a substantial improvement over $\mathcal{R}_1$ of 3.5%–10% absolute spherical coverage increase with hand reflections (corresponding to a relative improvement of 9%–16%). Thus, in this study, we see that the hand position/grip leads to a substantial performance decrease over the intended coverage of the subarray (akin to the hard hand grip case) but also a substantial performance increase over other regions of the

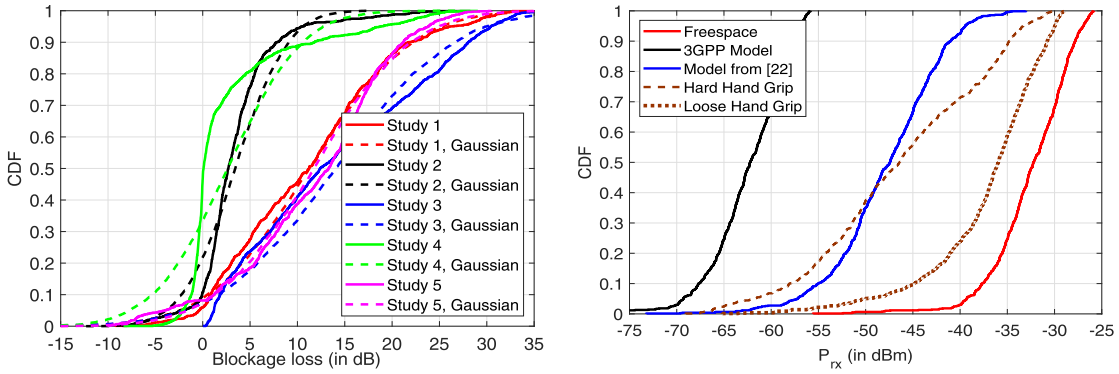

Fig. 9. (a) CDF of blockage loss with $\mathcal{R}_2$ in all the five studies. (b) $\mathsf{P_{rx}}$ comparison over the $\mathcal{R}_2$ RoI without and with different blockage models.

TABLE VII
STATISTICS OF BLOCKAGE LOSS IN THE FIVE STUDIES

Study	Gross loss estimate (in dB)	Relative % of sphere lost	Relative RoI improvement (in %)	Δ_2 (in dBm)	Mean (in dB)	Median (in dB)	Std. dev. (in dB)	% of sphere
1	8.6 to 17.2	66.7% to 85.3%	2.1% to 4.6%	-35	13.9	15.4	9.2	30.8%
2	3.6 to 10.6	36.0% to 43.9%	6.7% to 8.0%	-35	4.2	3.8	5.9	31.7%
3	15.9 to 19.7	90.8% to 100.0%	0% to 1.7%	-40	19.3	18.4	8.1	51.3%
4	0.4 to 10.8	20.0% to 25.7%	8.5% to 12.9%	-40	1.5	0.04	10.4	57.9%
5	9.5 to 12.7	68.6% to 99.9%	8.9% to 15.7%	-45	15.9	17.9	9.5	43.0%

sphere where the subarray is not intended to cover (akin to the loose hand grip case). This complementary behavior is possibly due to the orientation of the hand/fingers with respect to the antenna module with relatively bigger air gaps than the hard hand grip mode, but with body obstructing the signal as in the hard hand grip mode. Such aspects of blockage need to be carefully considered in understanding the implications of blockage in practical settings with the impact of the hand, fingers, and body separately understood. Some initial studies along this direction have been reported in [15]–[17].

V. MODELS FOR BLOCKAGE AND ITS IMPACT ON PHYSICAL LAYER PERFORMANCE

We now explore good stochastic model fits for signal strength changes with hand/body blockage and what these models imply for physical layer performance. At this point, some clarifications on the usage of stochastic models for blockage behavior in practice are necessary. In general, variables, such as hand grip, UE orientation, and the user's hand/body properties, lead to a deterministic impact on how strong/weak blockage loss is at any (θ, ϕ) angle pair. However, the intuition behind a stochastic model is that notions, such as a model on hand grips and hand/body properties, are not mature, and thus, we can break down hand grips into three coarse quantization classes (hard, intermediate, and loose hand grips) in this work. For each of these coarse quantization classes, based on representative measurement data as reported in Sections III and IV, we define an RoI where the impact of blockage is the largest and generate a stochastic model for the blockage behavior based on this RoI.

Toward this goal, Fig. 9(a) first shows the CDF of blockage loss defined as the signal strength difference between the without and with blockage scenarios in the five studies with $\mathcal{R}_2$ leading to the RoI in these studies. To augment Fig. 9(a), Table VII shows the statistics of blockage loss in these five studies along with the parameters that go into the RoI definitions. In addition to plotting the empirical loss data, a simple conditional Gaussian fit with the mean and standard deviation of the data conditioned on the choice of Δ_2 corresponding to the definition of $\mathcal{R}_2$ is also plotted for each of the five studies in Fig. 9(a). At this point, it is important to note that the model fits are with a conditional Gaussian distribution and not a Gaussian distribution. Thus, it is not a three-parameter model, but a two-parameter[5] model that is based on the choice of a third parameter that defines $\mathcal{R}_2$. It is important to note that the conditioning on Δ_2 is different for each study considered in this work.

Fig. 9(a) also shows that while simple conditional Gaussian models are good for hard/intermediate hand grips with substantial losses, looser hand grips with a steeper loss curve and wider tails need more sophisticated multiparameter model such as conditional Gamma distribution and conditional Weibull distribution [22]. Empirical fits of such distributions to data are the subject of ongoing work and will be reported elsewhere.

As mentioned earlier, we note that the mean of blockage loss is substantially less in all the five cases (even with the hard hand grip) relative to prior works that reported loss often in excess of 30 dB [7]–[9], [16], [17]. The sources of

[5]The subtle difference between a three-parameter model and a two-parameter model conditioned on a third parameter is the following. In a three-parameter model, the choice of the third parameter is unclear and we have to define the two other parameters for every choice of this third parameter. In the current setup, there is a certain good choice of the third parameter that defines the RoI $\mathcal{R}_2$ (namely, Δ_2), which depends on the context (e.g., hand grip, UE orientation, and hand/body properties) and conditioned on this choice of Δ_2, and we have a certain set of the two other parameters that capture the distribution of blockage loss.

discrepancies for such wide variations could include multiple factors. Some of these factors are given in the following.

1) *Beamwidth Differences Between Phased Array of Antennas in Commercial Form-Factor UEs Relative to Horn Antenna Studies That Have Been Reported in Prior Works:* For example, 4×1, 2×1 and 2×2 phased arrays are commonly used in commercial grade UEs with a beamwidth of beams made of progressive phase shifts being 25°–30° or 55°–60°. On the other hand, horn antennas at 28 GHz typically have a beamwidth between 10° and 15°. With a narrow range of angles over which energy can be collected, horn antenna studies with the human hand typically show far significant signal deterioration.
2) *Material Property Differences Between UEs and Horns:* Typical substrate material used in printed circuit board (PCB) planar antenna array design as well as the impact of circuitry associated with sensors, cameras, batteries, and so on could lead to polarization- and angle-dependent signal distortion [30]. This in turn leads to energy seeping into directions different from those intended for transmission/reception [13]. Thus, horn antenna-based studies typically capture a pessimistic view of the impact of hand and body blockage.
3) *Reflections Due to Hand That Is Often Unaccounted for in Prior Works:* The dimensions of the hand and fingers are typically more aligned with the form-factor UE design than with horn antennas leading to more reflections in unintended directions. By capturing a wider RoI (e.g., $\mathcal{R}_2$) than possible with $\mathcal{R}_1$, we are able to more accurately capture the impact of hand reflections on blockage behavior.

We now study the implications of blockage loss from the hand holding on beamforming performance relative to models from prior works. For this, Fig. 9(b) shows the P_{rx} distribution seen over the Freespace scenario and the hand holding in Studies 1 and 2 (hard hand grip versus loose hand grip mode) with the $\mathcal{R}_2$ RoI and by setting $\Delta_2 = -35$ dBm. Also, the P_{rx} deteriorations due to the 3GPP model [4] and the model from [22] for this RoI are plotted. Clearly, we note that the 3GPP model widely overestimates the blockage loss even in the hard hand grip case. On the other hand, the model from [22] has a comparable performance to the hard hand grip case, whereas it overestimates the blockage loss in the loose hand grip case. Even within the hard hand grip case, the model from [22] does not capture the hand reflections, and thus, there is a crossover between the CDFs observed here and the model from [22] (better true performance at peak coverage points and weaker true performance at lower tails). Such a crossover can lead to a poor estimation of EIRP (and thus physical layer performance) in a practical context, which requires careful study such as the one in this work.

VI. Conclusion

The focus of this article has been on understanding hand/body blockage with commercial quality phased arrays in a UE operating at 28 GHz. For this, five controlled studies were performed and the impact of blockage was estimated with hard, intermediate, and loose hand grips. Our studies showed that blockage produces a complex effect on the received signal strength depending on the direction of interest. In the main scenario (also addressed in prior works), blockage leads to signal strength deterioration. However, unlike estimates from prior works that are excessive, we show that this deterioration is moderate ($<$5 dB for loose hand grip) to reasonable ($<$15 dB for intermediate to hard hand grips). In addition, with looser hand grips and based on the hand holding, signals can be reflected by the fingers, palm, and different parts of the hand to improve signal strengths in hitherto weak signal directions (as seen from a no blockage perspective). Such a complicated behavior has not been explored or illustrated in prior works and this work documents such hand reflection gains.

In terms of future work, this article exposes the need for further careful studies in understanding how blockage can affect millimeter-wave devices. It is important to emphasize that the results presented in this article have been obtained from a single measurement campaign using different testing persons. While there are broad consistencies with prior blockage results using OTA measurements [22] across different research groups [10], [13], [18] and internal self-consistency across different array sizes (4×1 versus 2×1) that show a primary dependence on hand grips, more studies are needed to understand the representativeness of the data reported here. Another concern with this work is related to how the conclusions reported here may be extended to other antenna configurations. In this context, a theoretical explanation of the blockage findings would help with representativeness issues. While this article primarily focuses on the measurements aspects, we are currently investigating the theoretical aspects with a generalized form of the creeping wave theory in [13] tailored to form-factor device design that has been used to explain reduced blockage losses.

More studies are also needed to understand the impact of large array sizes on the expected increased blockage loss due to reduced beamwidths. Given that blockage is expected to have a serious effect on the link budget of commercial/cellular systems, a number of system-level design questions become pertinent. It is important to understand how different user hand grips/holdings can affect signal strength behavior (perhaps generating some parametric models to capture these effects), how blockage plays into network densification questions, and the role of mitigation mechanisms such as multipanel, multibeam, and cooperative schemes. Also, the cost–power–performance tradeoffs in the use of multiple antenna modules at millimeter-wave frequencies [19] are important to understand. Yet, another broad question of interest is the tuning of hand phantoms to match true hand holding results [1].

References

[1] V. Raghavan, M. A. Tassoudji, Y.-C. Ou, O. H. Koymen, and J. Li, "Impact of hand blockage on form-factor millimeter wave user equipment design," in *Proc. IEEE Asilomar Conf. Signals, Syst. Comput.*, Nov. 2020, pp. 1–5.
[2] A. Ghosh *et al.*, "Millimeter-wave enhanced local area systems: A high-data-rate approach for future wireless networks," *IEEE J. Sel. Areas Commun.*, vol. 32, no. 6, pp. 1152–1163, Jun. 2014.

[3] A. Maltsev *et al.* (May 2010). *Channel Models for 60 GHz WLAN Systems, doc: IEEE 802.11-09/0334r8*. [Online]. Available: https://mentor.ieee.org/802.11/documents

[4] *Technical Specification Group Radio Access Network; Study on Channel Model for Frequencies From 0.5 to 100 GHz (Rel. 14)*, document 3GPP TR 38.901 V14.3.0, Dec. 2017.

[5] METIS 2020. (Jul. 2015). *METIS Channel Model, Deliverable D1.4v3*. [Online]. Available: https://www.metis2020.com/wp-content/uploads/

[6] M. Peter *et al.*, "Analyzing human body shadowing at 60 GHz: Systematic wideband MIMO measurements and modeling approaches," in *Proc. 6th Eur. Conf. Antennas Propag.*, Prague, Czech Republic, Mar. 2012, pp. 468–472.

[7] G. R. MacCartney, Jr. *et al.*, "Millimeter-wave human blockage at 73 GHz with a simple double knife-edge diffraction model and extension for directional antennas," in *Proc. IEEE 84th Veh. Technol. Conf. (VTC-Fall)*, Montreal, QC, Canada, Sep. 2016, pp. 1–6.

[8] G. R. MacCartney and T. S. Rappaport, "A flexible millimeter-wave channel sounder with absolute timing," *IEEE J. Sel. Areas Commun.*, vol. 35, no. 6, pp. 1402–1418, Jun. 2017.

[9] G. R. MacCartney, T. S. Rappaport, and S. Rangan, "Rapid fading due to human blockage in pedestrian crowds at 5G millimeter-wave frequencies," in *Proc. IEEE Global Commun. Conf.*, Singapore, Dec. 2017, pp. 1–7.

[10] K. Zhao, J. Helander, Z. Ying, D. Sjöberg, M. Gustafsson, and S. He, "mmWave phased array in mobile terminal for 5G mobile system with consideration of hand effect," in *Proc. 81st IEEE VTC Spring*, Glasgow, U.K., May 2015, pp. 1–4.

[11] K. Zhao, J. Helander, D. Sjöberg, S. He, T. Bolin, and Z. Ying, "User body effect on phased array in user equipment for the 5G mmWave communication system," *IEEE Antennas Wireless Propag. Lett.*, vol. 16, pp. 864–867, 2017.

[12] K. Zhao *et al.*, "Channel characteristics and user body effects in an outdoor urban scenario at 15 and 28 GHz," *IEEE Trans. Antennas Propag.*, vol. 65, no. 12, pp. 6534–6548, Dec. 2017.

[13] I. Syrytsin, S. Zhang, G. F. Pedersen, K. Zhao, T. Bolin, and Z. Ying, "Statistical investigation of the user effects on mobile terminal antennas for 5G applications," *IEEE Trans. Antennas Propag.*, vol. 65, no. 12, pp. 6596–6605, Dec. 2017.

[14] B. Yu, K. Yang, C.-Y.-D. Sim, and G. Yang, "A novel 28 GHz beam steering array for 5G mobile device with metallic casing application," *IEEE Trans. Antennas Propag.*, vol. 66, no. 1, pp. 462–466, Jan. 2018.

[15] B. Xu *et al.*, "Radiation performance analysis of 28 GHz antennas integrated in 5G mobile terminal housing," *IEEE Access*, vol. 6, pp. 48088–48101, 2018.

[16] M. Heino, C. Icheln, and K. Haneda, "Finger effect on 60 GHz user device antennas," in *Proc. 10th Eur. Conf. Antennas Propag. (EuCAP)*, Davos, Switzerland, Apr. 2016, pp. 1–5.

[17] M. Heino, C. Icheln, and K. Haneda, "Self-user shadowing effects of millimeter-wave mobile phone antennas in a browsing mode," in *Proc. 13th Eur. Conf. Ant. Prop. (EuCAP)*, Krakow, Poland, Apr. 2019, pp. 1–5.

[18] J. Hejselbæk, J. Ø. Nielsen, W. Fan, and G. F. Pedersen, "Measured 21.5 GHz indoor channels with user-held handset antenna array," *IEEE Trans. Antennas Propag.*, vol. 65, no. 12, pp. 6574–6583, Dec. 2017.

[19] V. Raghavan, M.-L. (Clara) Chi, M. A. Tassoudji, O. H. Koymen, and J. Li, "Antenna placement and performance tradeoffs with hand blockage in millimeter wave systems," *IEEE Trans. Commun.*, vol. 67, no. 4, pp. 3082–3096, Apr. 2019.

[20] K. Zhao *et al.*, "Spherical coverage characterization of 5G millimeter wave user equipment with 3GPP specifications," *IEEE Access*, vol. 7, pp. 4442–4452, 2019.

[21] I. Syrytsin, S. Zhang, and G. F. Pedersen, "User impact on phased and switch diversity arrays in 5G mobile terminals," *IEEE Access*, vol. 6, pp. 1616–1623, 2018.

[22] V. Raghavan *et al.*, "Statistical blockage modeling and robustness of beamforming in millimeter-wave systems," *IEEE Trans. Microw. Theory Techn.*, vol. 67, no. 7, pp. 3010–3024, Jul. 2019.

[23] 3GPP Specification Series. (2017). *Technical Specifications, 38 Series*. [Online]. Available: https://www.3gpp.org/DynaReport/38-series.htm

[24] V. Raghavan, J. Cezanne, S. Subramanian, A. Sampath, and O. Koymen, "Beamforming tradeoffs for initial UE discovery in millimeter-wave MIMO systems," *IEEE J. Sel. Topics Signal Process.*, vol. 10, no. 3, pp. 543–559, Apr. 2016.

[25] S. Shakib, M. Elkholy, J. Dunworth, V. Aparin, and K. Entesari, "A wideband 28-GHz transmit–receive front-end for 5G handset phased arrays in 40-nm CMOS," *IEEE Trans. Microw. Theory Techn.*, vol. 67, no. 7, pp. 2946–2963, Jul. 2019.

[26] S. Shakib, J. Dunworth, V. Aparin, and K. Entesari, "mmWave CMOS power amplifiers for 5G cellular communication," *IEEE Commun. Mag.*, vol. 57, no. 1, pp. 98–105, Jan. 2019.

[27] V. Raghavan *et al.*, "Spatio-temporal impact of hand and body blockage for millimeter-wave user equipment design," *IEEE Commun. Mag.*, vol. 56, no. 12, pp. 46–52, Dec. 2018.

[28] V. Raghavan, S. Subramanian, J. Cezanne, and A. Sampath, "Directional beamforming for millimeter-wave MIMO systems," in *Proc. IEEE Global Telecommun. Conf. (GLOBECOM)*, San Diego, CA, USA, Dec. 2015, pp. 1–7.

[29] C. A. Balanis, *Antenna Theory: Analysis and Design*, 3rd ed. New York, NY, USA: Wiley, 2005.

[30] V. Raghavan, A. Partyka, L. Akhoondzadeh-Asl, M. A. Tassoudji, O. H. Koymen, and J. Sanelli, "Millimeter wave channel measurements and implications for PHY layer design," *IEEE Trans. Antennas Propag.*, vol. 65, no. 12, pp. 6521–6533, Dec. 2017.

Vasanthan Raghavan (Senior Member, IEEE) received the B.Tech. degree in electrical engineering from IIT Madras, Chennai, India, in 2001, and the M.S. degree in electrical and computer engineering, the M.A. degree in mathematics, and the Ph.D. degree in electrical and computer engineering from the University of Wisconsin, Madison, WI, USA, in 2004, 2005, and 2006, respectively.

He is currently a Senior Staff Engineer with Qualcomm, Inc., Bridgewater, NJ, USA. His research interests span multiantenna communication techniques, information theory, quickest change-point detection, and random matrix theory.

Sonsay Noimanivone is currently a Senior Support Engineer at Qualcomm, Inc., San Diego, CA, USA, with expertise on 5G over-the-air measurements for millimeter-wave systems. Over the last few years, he has worked on testing of multiple commercial millimeter-wave modem implementations.

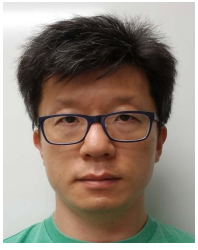

Sung Kil Rho is currently a Senior Support Engineer at Qualcomm, Inc., San Diego, CA, USA, with expertise on 5G over-the-air measurements for millimeter-wave systems. Over the last few years, he has worked on testing of multiple commercial millimeter-wave modem implementations.

Bernie Farin is currently a Staff Engineering Technician at Qualcomm, Inc., San Diego, CA, USA, with expertise on 5G over-the-air measurements for millimeter-wave systems. He has been involved in the design of 5G modem testing over the last few years.

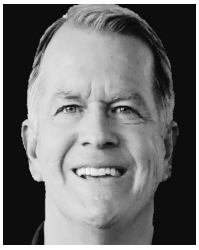

Patrick Connor received the B.S. degree in engineering and industrial technology from Cal State University, Long Beach, CA, USA, in 1990.

He is currently the Director of Hardware Systems at Qualcomm, Inc., San Diego, CA, USA. He has over 26 years of experience in antenna design and over-the-air (OTA) antenna test methodologies and he is the responsible system architect for multiple antenna lab test facilities at Qualcomm. He is also one of the lead antenna design engineers for Qualcomm's early commercial mobile devices, including 3GPP-compliant phone models. Prior to Qualcomm, he spent ten years at TRW Space and Technology, Cape Canaveral, FL, USA, where he performed antenna test measurements on spacecraft antenna systems, including satellite payload launch test activities.

Mr. Connor is an active member of the CTIA OTA Working Group and the RAN4 OTA Testability Working Group.

Ricardo A. Motos is currently a Staff Support Engineer at Qualcomm, Inc., San Diego, CA, USA, with expertise on 5G over-the-air measurements for millimeter-wave systems. He has been involved in measurements of commercial 5G modems, including hand and body blockage studies.

Yu-Chin Ou (Member, IEEE) was born in Taiwan. He received the Ph.D. degree in electrical and computer engineering from the University of California at San Diego, La Jolla, CA, USA, in 2011.

He joined Qualcomm, Inc., San Diego, CA, USA, in 2011. Since 2011, he has worked on millimeter-wave antenna design. He is a co-inventor of five granted U.S. patents.

Kobi Ravid received the B.S. degree in electrical engineering, the B.S. degree in physics, and the M.S. degree in electrical engineering–systems from Tel Aviv University, Tel Aviv, Israel, in 2004, 2004, and 2008, respectively.

He is currently a Senior Staff Engineer with Qualcomm, Inc., Bridgewater, NJ, USA. His primary research interests are in 5G/6G wireless system architectures, efficient radio frequency front-end designs, and system-level optimization.

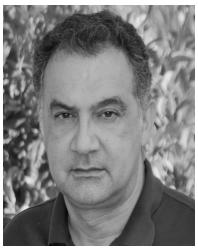

Mohammad Ali Tassoudji received the B.S. and M.S. degrees in electrical engineering from the University of Michigan, Ann Arbor, MI, USA, in 1987 and 1988, respectively, and the Ph.D. degree in electrical engineering from the Massachusetts Institute of Technology, Cambridge, MA, USA, in 1994.

Since graduation, he has been with Qualcomm, Inc., San Diego, CA, USA, where he is currently a Senior Director and is engaged in the research and development of antennas and systems.

Ozge Hizir Koymen (Member, IEEE) received the B.S. degree in electrical and computer engineering from Carnegie Mellon University, Pittsburgh, PA, USA, in 1996, and the M.S. and Ph.D. degrees in electrical engineering from Stanford University, Stanford, CA, USA, in 1997 and 2003, respectively.

He has been with the Corporate Research and Development Division, Qualcomm, Inc., Bridgewater, NJ, USA, since 2006, where he is currently a Senior Director working on 5G millimeter-wave access systems. He was earlier a member of Flarion Technologies, Bridgewater, developing OFDMA systems from 2003 to 2006. His prior experience includes consulting work for TRW, Los Angeles, CA, USA, from 1996 to 2000 and Impinj, Inc., Seattle, WA, USA, from 2000 to 2003.

Junyi Li (Fellow, IEEE) received the Ph.D. degree in electrical engineering from Purdue University, West Lafayette, IN, USA, in 1998, and the M.B.A. degree from the Wharton School, University of Pennsylvania, Philadelphia, PA, USA, in 2005.

He is currently the Vice President of Engineering at Qualcomm, Inc., Bridgewater, NJ, USA. He was a key inventor of Flash-OFDM, arguably the first commercially deployed OFDMA-based mobile broadband wireless communications system. He holds over 500 U.S. patents and has more than 600 pending patent applications. He was a Founding Member of Flarion Technologies, Bridgewater, a startup acquired by Qualcomm, Inc., in 2006. Prior to that, he was with Bell Labs, Lucent Technologies, Murray Hill, NY, USA. He is a coauthor of the book *OFDMA Mobile Broadband Communications* (Cambridge University Press).

Dr. Li received the Outstanding Electrical and Computer Engineers Award from Purdue University in 2012.